December 1, 1987

Electric field and plasmadensity measurements in the strongly-driven daytime equatorial electrojet: 2. Two-streamwaves

R. F. Pfaff
M. C. Kelley
E. Kudeki
Bela G. Fejer, *Utah State University*
K. D. Baker

JOURNAL OF GEOPHYSICAL RESEARCH, VOL. 92, NO. A12, PAGES 13,597–13,612, DECEMBER 1, 1987

Electric Field and Plasma Density Measurements in the Strongly Driven Daytime Equatorial Electrojet 2. Two-Stream Waves

R. F. PFAFF,[1] M. C. KELLEY,[2] E. KUDEKI,[3] B. G. FEJER,[4] AND K. D. BAKER[4]

Both primary and secondary two-stream (Farley-Buneman) waves have been detected by in situ electric field and plasma density probes in the strongly driven daytime equatorial electrojet over Peru. Simultaneous Jicamarca radar observations showed strong vertical and oblique 3-m type 1 echoes, also indicative of the two-stream mechanism. The rocket data show the two-stream region on the topside of the unstable layer to be situated between 103 and 111 km where the electron current was the strongest. This region was characterized by broadband plasma oscillations extending past 1 kHz in the rocket frame. Furthermore, above 106.5 km, where the electron density gradient was stable, a layer of laminarlike, horizontally propagating two-stream waves was detected. These waves were strongest near 108 km, the altitude where previous measurements have shown the electrojet current over Peru to be strongest. The peak rocket frame frequency of these waves was 25 Hz, and the observed broadband electric field and plasma density amplitudes were 2 mV/m and 1–2% rms, respectively. The electric field amplitudes were likely attenuated by a spatial filtering effect and may have been several times higher. The data suggest that these waves had phase velocities comparable to the electron drift velocity ($\simeq$ 500 m/s) and peak wavelengths (2–3 m) that agree with kinetic theory predictions. Distinct vertically oriented waves which may have been generated by a mode coupling process were also observed by the rocket in this region, in agreement with the simultaneous radar observations. Below the laminar two-stream layer, in the region of the large-scale, gradient drift driven horizontal electric fields, secondary two-stream waves were observed that were driven by localized $\delta\mathbf{E} \times \mathbf{B}$ plasma drifts. The amplitudes of the horizontally propagating kilometer scale waves were clearly strong enough (10–15 mV/m) to drive vertically oriented secondary two-stream (type 1) waves, as proposed by Sudan et al. (1973) and observed by the Jicamarca radar between roughly 103 and 106 km. Below 103 km, secondary two-stream waves could not be generated because ψ (the ratio of the ion and electron collision frequencies to their gyro frequencies) becomes large, despite the fact that the observed large-scale wave amplitudes remained strong at the lower altitudes. Observations of "flat-topped" waveforms of the large horizontal electric field structures suggest that secondary two-stream phase velocities may be saturated because of a limitation of the driving electric fields rather than a process intrinsic to the two-stream instability itself.

1. INTRODUCTION

The collisional two-stream instability was first developed by *Farley* [1963], using kinetic theory, and *Buneman* [1963], using the fluid equations, principally as a means of explaining radar observations of 3-m irregularities in the electrojet over Peru. Their work established that in cases where components of the relative electron-ion drift velocity exceed a threshold roughly equivalent to the ion sound speed, electrostatic meter scale waves will be generated in an unstable two-dimensional cone in the plane perpendicular to the magnetic field and centered upon the direction of the local plasma drift. In the intervening years the two-stream mechanism has undergone considerable theoretical development. For example, the theory has been developed to include the effects of a stabilizing or destabilizing electron density gradient [e.g., *Rogister and D'Angelo*, 1970; *Sudan et al.*, 1973; *Schmidt and Gary*, 1973], parallel propagation effects [e.g., *Lee and Kennel*, 1973; *Ossakow et al.*, 1975], and strongly driven plasma conditions as are common in the auroral zone [e.g., *Lee et al.*, 1971]. In addition, *Sudan et al.* [1973] developed the ideas that two-stream waves may also be generated via a two-step process, in which the driving plasma drift may be governed by that due to a large-amplitude wave electric field. Although in principle this mechanism still involves linear theory, this work was important in explaining radar observations of two-stream waves perpendicular to the current flow and for developing early ideas of plasma turbulence in the electrojet.

Considerable theoretical attention has also been applied toward explaining several experimental characteristics of two-stream waves that cannot be explained with the linear theory. In particular, backscatter radar measurements of "saturated" phase velocities remain an intriguing aspect of the two-stream observations (see review by *Fejer and Kelley* [1980]), and some of the theories invoked to explain them include nonlinear orbit diffusion process [e.g., *Dupree*, 1966; *Sleeper and Weinstock*, 1972], quasi-linear mechanisms whereby the waves reduce the driving field [e.g., *Rogister*, 1971; *Sato*, 1972], and anomalous diffusion mechanisms that alter the local effective collision frequencies [*Sudan*, 1983*a*]. The theories of *Sudan* [1983*a*, *b*] have also been important for developing ideas concerning the evolution of two-stream waves in fully developed plasma turbulence. Further, the plasma heating that may result from the turbulent wave electric fields in the ionosphere has been discussed in a series of papers [*St.-Maurice et al.*, 1981; *St.-Maurice and Schlegel*, 1983; *St.-Maurice and Laher*, 1985; *St.-Maurice et al.*, 1986]. The current picture of theoretical research involving two-stream waves in the equatorial electrojet has recently been reviewed by *Farley* [1985].

Most of the experimental work concerning ionospheric two-

[1]Laboratory for Extraterrestrial Physics, NASA Goddard Space Flight Center, Greenbelt, Maryland.
[2]School of Electrical Engineering, Cornell University, Ithaca, New York.
[3]Aeronomy Laboratory, University of Illinois, Urbana.
[4]Center for Atmospheric and Space Sciences, Utah State University, Logan.

Paper number 7A9029.
0148-0227/87/007A-9029$05.00

stream waves has been carried out using coherent backscatter radars, whereas in situ observations, by comparison, have been relatively few. Laboratory observations of collisional two-stream waves have also been important in the study of many of the instability characteristics [e.g., *D'Angelo et al.*, 1974; *John and Saxena*, 1975].

Radar observations have established the existence of two-stream irregularities in both the equatorial and auroral electrojets (see review by *Fejer and Kelley* [1980]). In the equatorial region the principal radar characteristics of two-stream waves include narrow spectral widths, Doppler shifts corresponding to velocities near the acoustic velocity, the invariance of these Doppler shifts with elevation angle, a peak in the intensity of the two-stream radar echoes in the direction of the horizontal electrojet current, and an asymmetry evidence in the strength and occurrence of upgoing and downgoing two-stream radar echoes. These characteristics are reviewed by *Farley* [1985].

Electric field probes on board sounding rockets have parameterized two-stream waves in the auroral zone in several cases [e.g., *Kelley and Mozer*, 1973; *Pfaff et al.*, 1984]. In the equatorial region, however, in situ observations of two-stream waves have been far less definitive, primarily because of the smaller number of rocket experiments flown during strong electrojet conditions, the larger uncertainties at the equator introduced by typical vehicle Doppler shifts, and the lack of simultaneous radar data. Examples of in situ measurements related to the two-stream instability in the equatorial electrojet have been reported by *Prakash et al.* [1971, 1972] and *Smith and Royrvik* [1985]. *Pfaff et al.* [1985] reported in situ electric field observations from the Antarqui campaign in Peru in 1975 that were carried out during the presence of weak type 1 (two-stream) radar echoes recorded at Jicamarca. On the basis of the relatively weak in situ current measurements, those authors argued that the radar echoes must have been created by secondary two-stream waves driven by gradient drift wave electric fields, although these two-stream waves did not appear definitively in the in situ data.

This paper presents electric field and plasma density observations of both primary and secondary two-stream waves in the strongly driven daytime equatorial electrojet during the Condor campaign in Peru. The data were taken while simultaneous radar observations of two-stream waves were being carried out at Jicamarca and at Ancon, Peru. The radar observations are discussed in detail by *Kudeki et al.* [this issue], hereafter referred to as paper 1, and bear directly on the in situ measurements reported here. The rocket instrumentation description, in situ data overview, and long-wavelength (gradient drift) observations are presented in a second companion paper, *Pfaff et al.* [this issue], hereafter referred to as paper 2. In this work (paper 3) the in situ data pertaining to the two-stream observations are presented first, followed by a discussion of the results in terms of their linear and nonlinear theoretical implications.

2. DATA PRESENTATION

Primary Two-Stream Wave Observations

Introduction. As discussed in paper 2, a Taurus-Orion sounding rocket (vehicle number 33.027) was launched at 1034:36 (LT) on March 12, 1983, from Punta Lobos, Peru, along a westward trajectory parallel to the magnetic dip equator, attaining an apogee of 128 km. Instrumented with electric field and plasma density experiments, the payload was designed to study plasma irregularities in the equatorial electrojet. The rocket was launched in the presence of strong type 1 (two-stream) radar echoes as well as strong kilometer scale, horizontally propagating large-scale waves (see paper 1). The ΔH magnetometer deflection measured at Huancayo during launch was approximately 140 γ above the background level, indicative of a strong electrojet current overhead.

As shown in the electric field sonograms in paper 2, the in situ wave data displayed a well-defined layer of broadband oscillations extending past 1 kHz between 103 and 111 km on both the upleg and downleg traversals of the electrojet region by the rocket probes. Furthermore, the height interval of these waves was shown to agree with that region predicted to be unstable to the two-stream process based on linear theory.

Embedded in this layer of high-frequency waves, a well-defined coherent packet of low-frequency waves was also detected in the in situ electric field data. These waves were strongest between roughly 107 and 109 km and were observed on both the upleg and the downleg. We begin our analysis of the in situ two-stream observations with an investigation of these topside coherent waves. Since these low-frequency waves appeared at the altitude where the electrojet current is believed to be strongest and since the electron density gradient was stable in this region, we will argue that these waves represented a laminarlike layer of "pure" primary two-stream oscillations. Further, we will show that their low rocket frame frequency was a consequence of a severe Doppler shift resulting from the fact that the component of the vehicle velocity along the direction of propagation was comparable to the wave phase velocity.

Evidence of primary two-stream waves. One component of the dc-coupled horizontal electric field observed at 108 km in the topside two-stream region is shown in the upper panel of Figure 1. The large sine wave in the time series corresponds primarily to the $\mathbf{V} \times \mathbf{B}$ fields induced by the rocket's velocity $\mathbf{V}$, through the Earth's magnetic field $\mathbf{B}$, and is modulated at the rocket spin period (roughly 0.7 s). The smaller-amplitude sinusoidal variations superimposed on the large sine wave represent the primary two-stream waves that we wish to investigate. Since these data were observed on the upleg, the horizontal components of the $\mathbf{V} \times \mathbf{B}$ fields measured by this probe were oriented in the geomagnetic westward direction. Notice that the two-stream waves appeared at the crests of the large $\mathbf{V} \times \mathbf{B}$ signal. Since the $\mathbf{V} \times \mathbf{B}$ field is perpendicular to $\mathbf{B}$ and the rocket spin axis was within 10° of the vertical direction, this is a clear indication that these fluctuations had wave vectors in the plane perpendicular to the magnetic field. This result was also shown in the analysis of the twice-per-spin wave modulation using the gyro (attitude) data in paper 2.

The power spectral density distribution of the waves is shown in the lower panel of Figure 1 and reveals a spectral peak centered near 25 Hz. This enhancement corresponds to the distinct feature at 108 km apparent in the sonogram presented in Plate 1 of paper 2. The large contribution to the spectral power at frequencies below about 5 Hz in the spectrum in Figure 1 was due to the $\mathbf{V} \times \mathbf{B}$ sine wave at the spin rate of 1.4 Hz. The dc electric field analysis showed no significant wave power present at the lowest frequencies in this region, and it is clear that the falloff in power below roughly 15 Hz in the dc-coupled spectrum was real. At high frequencies the spectrum was extended using data from a separate band-pass channel on board the rocket. The spectral

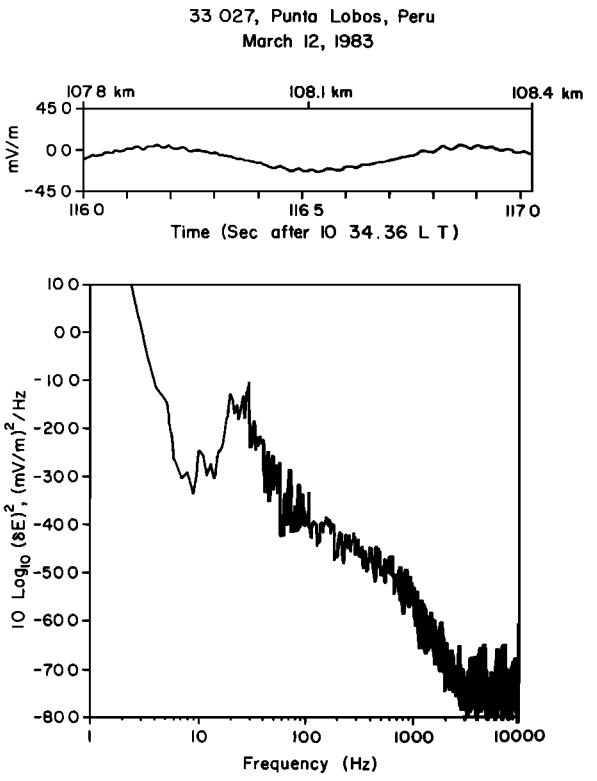

Fig. 1. Electric field observations of primary two-stream waves observed at 108 km on the upleg. The top panel shows the two-stream waves superimposed on the large-amplitude sine wave due primarily to $\mathbf{V} \times \mathbf{B}$. The bottom panel shows the power spectrum of this waveform merged with one computed from a separate, high-frequency band-pass detector of the same electric field component. The low-pass filter of the band-pass channel was 31 kHz.

"break" or "knee" near 800 Hz in the power spectrum will be discussed later on.

We now wish to establish the orientation of the enhanced packet of two-stream waves near 25 Hz in the plane perpendicular to the magnetic field, their principal wavelengths, their phase velocity, and the relationship between δE and $\delta n/n$ of the primary wave vectors.

Primary wave vector orientation. Although the observed two-stream electric field wave amplitudes maximized when the double-probe baseline was oriented in the magnetic east-west direction, this observation alone does not establish the propagation direction of the waves. (Since these are electrostatic waves, we assume $\delta\mathbf{E} \parallel \mathbf{k}$.) Indeed, waves in the plane perpendicular to the magnetic field but oriented in an oblique (non-horizontal) direction would also show a twice-per-spin modulation each time a horizontal electric field probe, spinning about the vertical direction, rotated into the plane perpendicular to the magnetic field.

In order to resolve this dilemma, we examined the electric field measurements from diagonally oriented sensors during a complete rocket spin cycle, since the measured wave electric fields should be consistent with the changing angle between the wave propagation direction and the spinning detector orientation. A diagonal detector mounted on a vertically spinning rocket at the magnetic equator would have substantially different relative orientations with respect to the direction of propagation of oblique waves than for horizontal waves during a complete spin cycle. (This assumes that the amplitude and direction of the waves are constant within a spin cycle.) *Temerin and Kelley* [1980] applied a similar procedure to measurements made with a skewed double probe of auroral zone VLF hiss in order to determine whether these waves were polarized parallel or perpendicular to the magnetic field direction.

The upper panel of Figure 2*a* shows the coherent two-stream waves discussed above measured by the diagonally oriented pair of sensors labeled 1 and 4 on the electric field double-probe diagram shown in Figure 2 of paper 2. For comparison, the same waves detected by the horizontal pair of sensors labeled 1 and 2 in that figure are shown in Figure 2*b*. The primary two-stream waves we are considering are those to the right of the arrow at 114.3 s. The components of the boom lengths of each detector along the magnetic equator are shown in the lower panels. A comparison of the absolute values of the amplitudes of these waves detected by the two sets of double probes is also significant, and we will return to it later. For now, we are concerned with the modulated envelope of these waveforms.

Notice that the maximum wave potentials measured between the diagonally oriented sensors 1 and 4 were roughly the same twice per spin when their measurement component perpendicular to the magnetic field was also maximum. This response is consistent with wave vectors that were primarily oriented along the magnetic equator. A more detailed examination shows a slight tendency for the wave amplitudes to be increased when this component of the diagonal measurement had reached its maximum negative excursion once per spin, a result consistent with a vertical driving electric field that had a

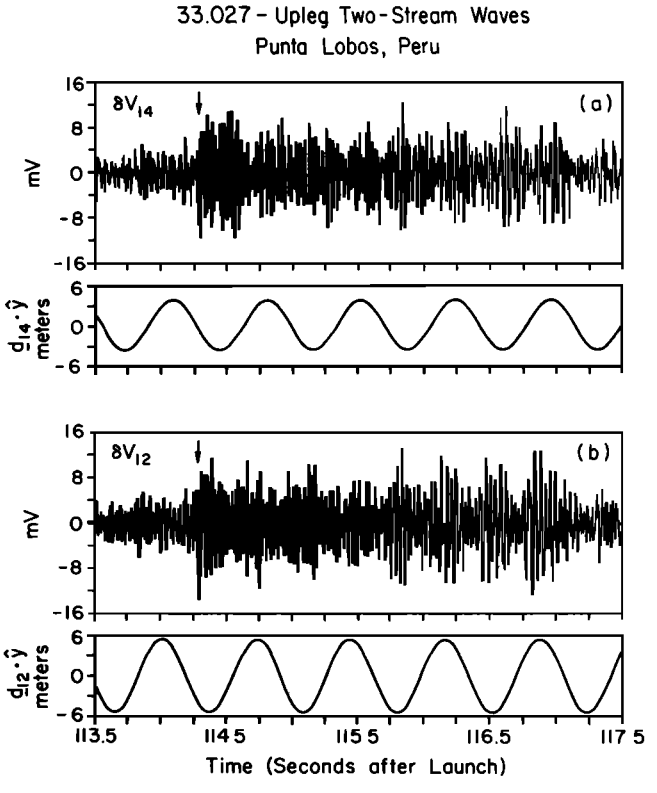

Fig. 2. Electric field wave observations detected by the diagonal δE_{14} and horizontal δE_{12} sensors. The low- and high-frequency roll-offs for these channels were 16.5 Hz and 940 Hz. The lower panels show the component of the measurement direction projected on the direction of the magnetic equator, $\hat{y}$.

small eastward component. The precise electric field double-probe response also depends on the small tilt of the rocket axis and on a spatial attenuation created by the fact that the wavelengths were comparable to the double-probe boom length components.

The general result of the above analysis is that the strongest two-stream waves were mainly propagating in a direction along the magnetic equator, as expected for primary waves driven by the horizontal electrojet current. This conclusion agrees with backscatter radar observations that show the cross section of two-stream waves strongly maximizes in the direction of the current [*Ierkic et al.*, 1980].

Wavelength and phase velocity. We now address the question of determining the principle wavelength and the phase velocity of the primary two-stream waves. Given the observed wave frequency ω_{obs} and assuming only one principal k direction, we wish to solve the following expression:

$$\omega_{obs} = \mathbf{k} \cdot \mathbf{V}_R - \mathbf{k} \cdot \mathbf{V}_\phi - \mathbf{k} \cdot \mathbf{U}_N \quad (1)$$

where $\mathbf{V}_R$ is the rocket velocity, V_ϕ is the phase velocity (which is always parallel to $\mathbf{k}$), and $\mathbf{U}_N$ is the neutral wind velocity. We shall call the total Doppler-shifted velocity of the waves in the rocket frame, $\mathbf{V}_{Dopp}$.

The wave vector direction corresponding to the waves in the spectral peak was established above to be primarily in the direction of the magnetic equator. The rocket velocity component in this direction was 482 m/s, and the neutral wind, based on the Jicamarca data, was roughly 80 m/s eastward (see paper 1). Now we must either determine the wavelength (which is invariant to the Doppler shift) and solve (1) for the phase velocity or determine the phase velocity and solve (1) for the wavelength.

The clearest observational evidence of the phase velocity and wavelength of the primary two-stream waves appeared from an examination of the frequency at which the instability was observed to "switch on." We can safely assume that this onset occurred at a phase velocity equal to the acoustic velocity.

The instability onset of the primary two-stream waves is depicted explicitly in the data in Figure 3. In the lower two panels of this figure the dc-coupled perpendicular spin plane measurements are shown. Again, the two-stream waves appeared as the smaller-amplitude sine waves superimposed on the large sine wave at the spin frequency which was due primarily to $\mathbf{V} \times \mathbf{B}$. In the panel immediately above, we have taken the sum of the squares of these two channels and subtracted the calculated $\mathbf{V} \times \mathbf{B}$ offset in the same manner performed in the analysis of the large-scale wave observations in paper 2. Notice that the initial burst of higher-frequency two-stream waves occurred precisely where a sharp discontinuity in the horizontal dc electric field was observed, indicating a reversal between the eastward and westward field directions (see arrow). We speculate that the local polarization (vertical) electric field was modulated by the changing horizontal field, and in this case, we hypothesize that it increased with the appearance of the eastward field to a value large enough such that the driving conditions for the two-stream instability were met.

The frequency of the two-stream waves in the rocket frame is revealed in the sonogram in the uppermost panel of Figure 3, which was computed from the time series representing the sum of the squares of the electric field components. The two-stream waves appear as the strong feature at 72.4 Hz (f_1) beginning at 114.27 s (see arrow), which then decreased in frequency to 22.1 Hz (f_2) at 117.0 s.

Let us now assume that when the waves "turned on" at 114.27 s, they were propagating at the acoustic velocity. This velocity was estimated from the Jicamarca data to be roughly 380 m/s, which corresponds to an electron temperature of approximately 260°, which is certainly reasonable. Combining this velocity with the component of the vehicle velocity along the magnetic equator and the neutral wind velocity, we find that the Doppler-shifted velocity $\mathbf{V}_{Dopp}$ at f_1 was 182 m/s. Thus, using (1), the wavelength of the peak in the spectrum was roughly 2.5 m. This result is in excellent agreement with linear kinetic theory (see section 3). We now further postulate that the change in the observed frequency with increasing time corresponded primarily to a change in the wave phase velocity and not to a change in the primary wavelength or neutral wind speed. Thus for propagation along the equator between 116 and 117 s at 108 km, for $f_2 = 22.1$ Hz, and for the same principle wavelength, $\mathbf{V}_{Dopp}$ becomes 56 m/s. The phase velocity of these waves in the neutral frame would then be 506 m/s.

We can also assume that the phase velocity of the waves was fixed at the acoustic velocity of 380 m/s and that the observed change was due to a change in wavelength. In this case, using (1), the dominant wavelength corresponding to the frequency of the peak at 116–117 s would then be 8.2 m. Since linear kinetic theory predicts that driving two-stream waves more strongly will shift the peak wavelength to shorter values [e.g., *Lee et al.*, 1971], this approach appears less likely to explain our observations.

We must also allow for changes in the neutral wind. The only available measurement of this value, from the Jicamarca Observatory, did not provide information concerning the variation of this parameter with height. However, it appears unlikely that the neutral wind velocity changed by over 100 m/s in roughly 2 km of altitude, at precisely the values needed to make the observations consistent with the constant acoustic velocity theory. Still, a combination of several changing parameters including wavelength, phase velocity, electron temperature, and neutral wind may have actually created the observed frequency variation.

To summarize the analysis so far, the sudden onset of the instability on the upleg at 106.7 km and the changing spectral features of the observed two-stream waves can be interpreted as the "switching on" of the primary instability when the threshold conditions were satisfied and as a change in the phase velocity of the waves. In this case, the data imply that the waves sped up on the topside of the electrojet, even though their measured frequency decreased. This occurred because the faster waves were Doppler-shifted into nearly the same frame of reference as that of the rocket. The principal wavelength of the waves using this procedure was 2–3 m. We note, however, that the observed phase velocities did not appear to slow down on the very topside, where presumably the drift velocity must weaken. As will be mentioned in section 3, this fact indicates that there are several aspects of the phase velocity analysis that we do not yet understand.

Two other independent methods were also investigated to deduce the phase velocity and wavelengths of the waves, although their results were even less definitive. One attempt sought to identify resonant interference patterns [e.g., *Temerin*, 1978] in the frequency-time sonograms of the two-stream

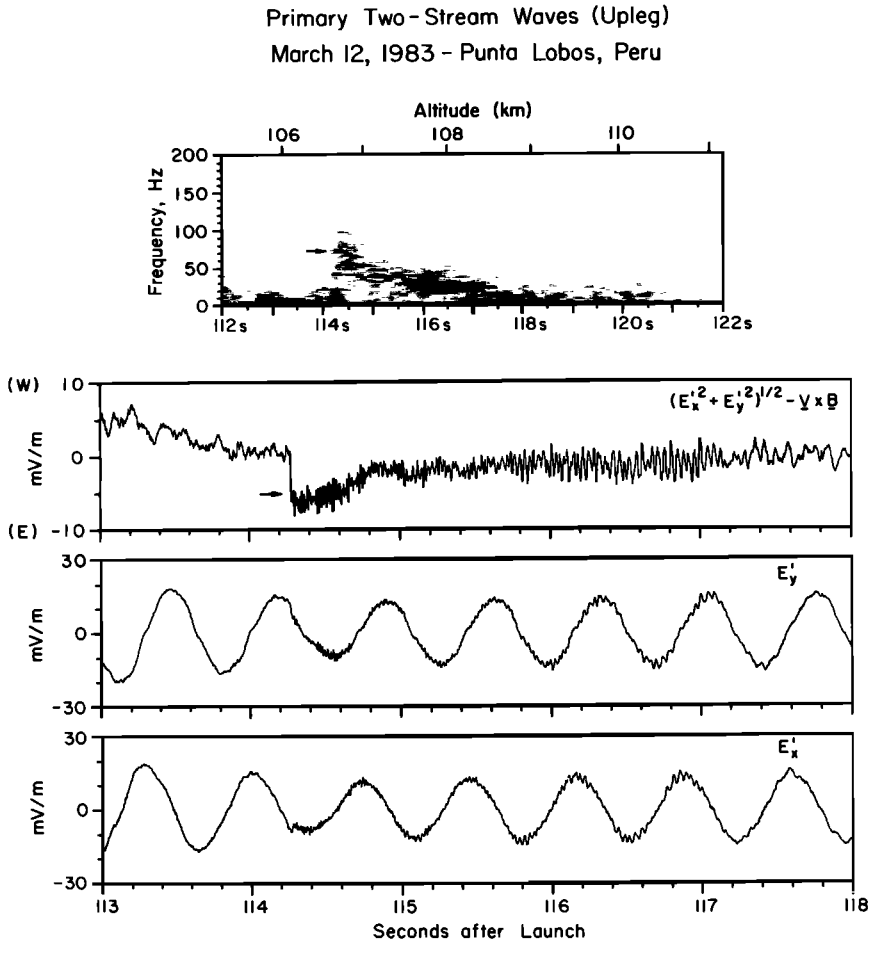

Fig. 3. Electric field observations of the primary two-stream waves for the upleg. The lower panels show two perpendicular components of the raw dc-coupled data, above which is plotted the square root of the sum of the squares of these waveforms, following the guidelines outlined in paper 2. The top panel shows a sonogram of these waves. (Note the change in the scale of the time axis.) An arrow indicates the onset of the strong burst of two-stream waves.

electric field data, which would be expected for laminar oscillations with wavelengths less than the 5.5-m double-probe separation distance. Another procedure involved a spaced-receiver measurement of the phase shift between waveforms measured by two sets of double probes offset in the horizontal direction, which would then yield the Doppler-shifted phase velocity and wavelength [e.g., *Bahnsen et al.*, 1978; *Kintner et al.*, 1984]. Both of the techniques were limited by the relatively high spin rate and short time series available, since the analysis in each case requires a high spectral resolution (i.e, long time series) on short data segments within the spin cycle. In addition, the fact that the waves were Doppler-shifted to very low frequencies also necessitated a high spectral resolution to adequately carry out these procedures. The results using these methods were not conclusive, although they did not preclude the wavelength and phase velocity results deduced from the analysis of the instability onset discussed above. The details of these other analyses are presented by *Pfaff* [1986].

Amplitudes of the wave electric fields. The potential Φ of an electrostatic wave measured by an electric field double probe is given by

$$\Phi = -\mathbf{d} \cdot \delta\mathbf{E}(k) \frac{\sin(\mathbf{k} \cdot \mathbf{d}/2)}{(\mathbf{k} \cdot \mathbf{d})/2} \quad (2)$$

where $\mathbf{d}$ is the baseline measurement vector. Since the dominant two-stream wavelengths were most likely smaller than the sensor separation distance (5.5 m), the wave amplitudes were spatially attenuated by the factor on the far right-hand side of (2). Using the principle wavelengths derived above, this attenuation can be unfolded from the power spectral densities of the two-stream waves. We will see that the computed correction factor for this effect is significant.

Another representation of the electric field observations of the two-stream waves is shown in Figure 4. The raw data, shown at the top of the figure, represent 71% of the spin cycle centered upon the magnetic equator. The measured potentials have been divided by the boom length of 5.5 m in this presentation. The variation of the wave amplitude is primarily due to the changing orientation of the double probe, $\mathbf{d}$, with respect to $\delta\mathbf{E}$ (or to $\mathbf{k}$).

The electric field wave spectrum is shown in the lower left panel in Figure 4. We wish to integrate the amplitudes over a certain band of frequencies (or wave numbers) and correct for the k^{-2} artificial attenuation in power for wavelengths shorter than $\lambda \simeq 2d$, as given by (2). We have assumed that the interference nulls discussed above were filled by the effects of the vehicle spin such that the sin $(\mathbf{k} \cdot \mathbf{d}/2)$ term in (2) is taken to be approximately 1, as shown by *Pfaff* [1986]. In this manner, the

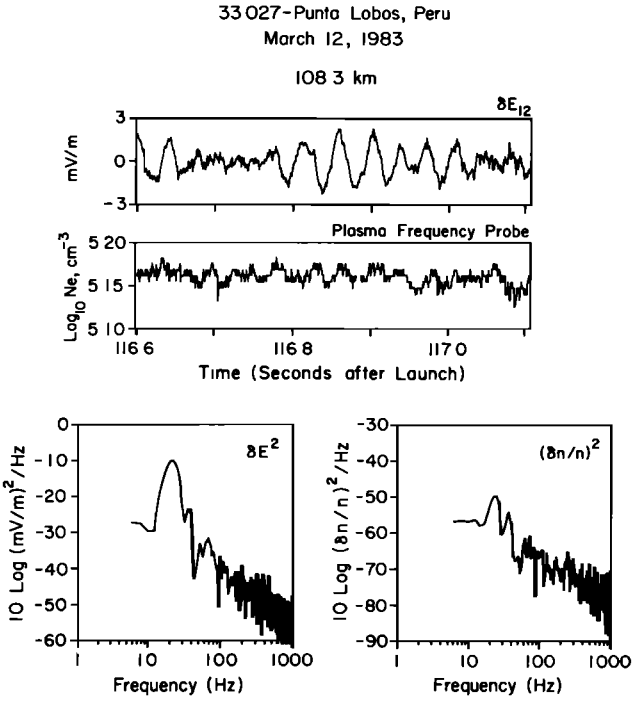

Fig. 4. Comparison of electric field and plasma density observations of two-stream waves on the upleg. The high-pass filter in the electric field data (3 dB at 16.5 Hz) has been unfolded in the electric field spectrum. The spectral estimates were smoothed with a three-point sliding average.

amplitude of a short-scale wave is attenuated by $\lambda/\pi d$. For example, for $\mathbf{d} \parallel \mathbf{k}$ where $|\mathbf{d}| = 5.5$ m and for a wavelength of 2.25 m, the wave amplitude would be attenuated from their true values by a factor of 7.7. Using a phase velocity of 506 m/s (with no spread in the amplitude or direction of V_ϕ assumed), the band of frequencies corresponding to the spectral peak from 15 to 45 Hz corresponds to wave numbers between 1.7 and 5.4 m^{-1}. The measured integrated electric field amplitude in this band is 1.0 mV/m rms. Using (2), this integrated amplitude equals 7.3 mV/m rms.

Clearly, the uncertainty surrounding the estimate of the attenuation factor is large. A more direct approach to estimating the wave electric fields would be to compare data taken from two baselines with different lengths, preferably parallel to each other, with at least one baseline or boom length short in comparison to the primary wavelength. On this payload, electric field data were taken both within the spin plane–sensor separation distance of 5.5 m and between the diagonally separated sensors whose component in the spin plane was 3.89 m. The voltages corresponding to the two-stream waves measured by these detectors were roughly the same, as shown in Figure 2, suggesting that the principal wavelengths were of the order of these distances, or smaller. If the wavelengths were at least twice as long as both the double-probe lengths, the measured voltages would be expected to simply scale with d, since then $\Phi = \mathbf{d} \cdot \delta\mathbf{E}$. The comparison of the amplitudes from the two detectors was actually fairly complicated, not only because the sin $(\mathbf{k} \cdot \mathbf{d}/2)$ term was different in each case but also because the diagonal detector was more susceptible than the spin plane detector to contributions from oblique and vertical wave vectors. Nevertheless, the above comparison is consistent with our analysis that the measured oscillations corresponded to principal wavelengths of a few meters.

Comparison of δE and $\delta n/n$. We now investigate the perturbations in plasma density associated with the two-stream waves and relate this measurement to the potential differences that we have just discussed. The most reliable measurement of the density perturbation of the waves was from the plasma frequency probe [*Baker et al.*, 1985]. Fortuitously, because the rocket was traveling at almost (but not quite) the same velocity as the waves, there was adequate time for the instrument to lock onto the local upper hybrid frequency within the crests and troughs of the meter scale waves, from which the local plasma density was determined.

The data from this instrument are also presented in Figure 4. The two-stream waves are the oscillations in the density waveform which appear just above the level imposed by the least significant bit. These raw data show peak amplitudes of roughly $\pm 2.5\%$. A power spectrum of the density data is shown in the lower right panel of Figure 4. Note the similarity between the coherent spectral peak measured by the δE and δn detectors. Using the same phase velocity estimate discussed above, the integrated density fluctuation amplitude between k values of 1.7 and 5.4 m^{-1} was $\pm 1.1\%$ rms. In section 3 we will compare the measured ratio of $\delta E/E$ to $\delta n/n$ with that predicted theoretically.

Although the phase difference between the δE and $\delta n/n$ waveforms is also of interest, attempts to compute this value from these data did not produce reliable results because of the large phase shift (roughly 90°) near the frequencies of interest inherent in the transfer function of the electric field receiver.

Short Vertical Waves in the Two-Stream Region

So far, we have been dealing with the large-amplitude spectral peak which appeared between 15 and 50 Hz near 108 km altitude. Now we consider the higher-frequency waves associated with the two-stream region that were first encountered in the sonograms shown in Plate 1 and Figures 4*a* and 4*b* in paper 2.

The high-frequency component of the waves in the two-stream region are shown in expanded sonograms in Figures 5*a* and 5*b* of this paper for the upleg and downleg. The gray levels have been enhanced to emphasize the high-frequency waves. Notice the distinct twice-per-spin modulation between roughly 100 and 800 Hz on the topside of the irregularity layer for both the upleg and downleg measurements. At first glance, these high-frequency waves appear to be extensions of the primary two-stream spectrum which we have just discussed and which also showed a distinct twice-per-spin modulation. However, whereas the amplitude of the lower-frequency, narrowly peaked waves maximized when the boom rotated into the plane perpendicular to the magnetic field, this twice-per-spin modulation does not show this same dependency.

To illustrate this, we compare the peaks of the high-frequency waves with the orientation of the double probe within the spin cycle. The upper panels of Figures 5*a* and 5*b* show power profiles calculated from the spectra displayed in the sonograms below. In the upleg data, notice that the peaks in the higher-frequency power occurred roughly 90° out of phase with the peaks in the low-frequency power. In the downleg data, however, the modulation of the high-frequency waves occurs in a different location in the spin cycle (in this case, roughly when the boom was aligned with the east-west

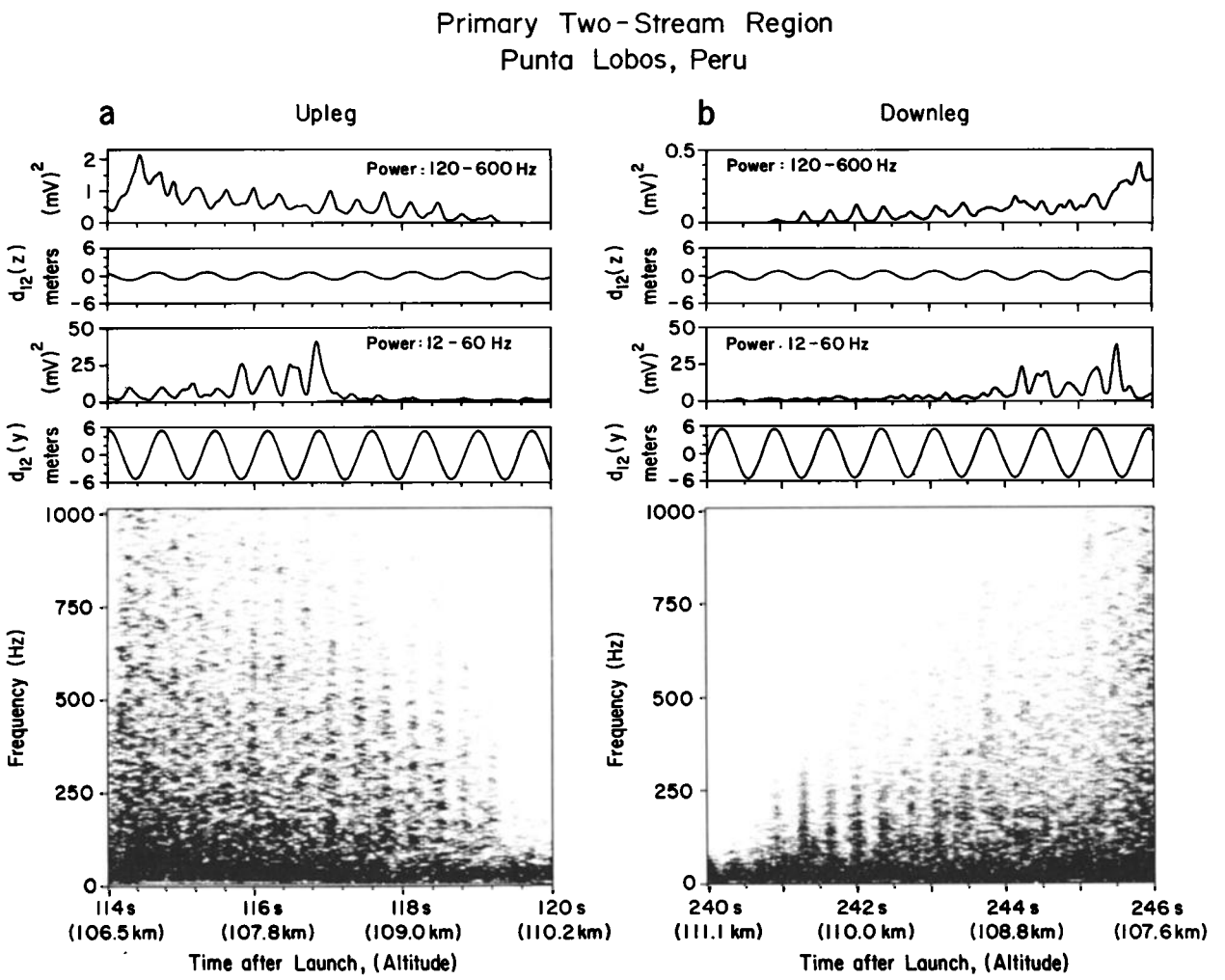

Fig. 5. Sonograms and integrated power plots of the electric field oscillations observed in the "pure" two-stream region on the (*a*) upleg and (*b*) downleg. The gray levels in the sonograms have been selected to show the high-frequency twice-per-spin modulation.

direction). As discussed earlier, note that the twice-per-spin modulation does not necessarily indicate that the wave vectors were aligned with the double probe at the times of the peak signals, only that $|\mathbf{d} \cdot \mathbf{k}|$ was maximum at these times. One explanation to account for the observed high-frequency twice-per-spin modulation, which can explain both the upleg and the downleg data, comes into view if we consider that these waves propagated in the vertical direction.

In order to correctly interpret the high-frequency spin-modulated waves, we must consider the precise attitude of the payload while it was in the topside, "pure" two-stream region. As shown in Figure 6*a*, the payload was pitched at an angle of 10° down toward the magnetic field for this portion of its flight on the upleg. Thus when the component of the boom along **B** was maximized twice during each spin cycle, its component in the vertical direction was maximized as well. If the higher-frequency waves were due to vertically propagating waves, their amplitudes would peak when the vertical component of the boom also peaked. This relationship is exactly what was observed, as can be seen by comparing the component of the boom in the vertical direction ($d_{12}(z)$) with the power profiles in Figure 5*a*. For the downleg data the payload was in a different position in its coning cycle, as shown in Figure 6*b*. Notice that the peaks in the high-frequency wave power on the downleg, shown in the top panel of Figure 5*b*, also correspond to the maxima in the vertical component of the spinning double probe. The fact that the observed high-frequency oscillations "tracked" the coning of the rocket in this fashion strongly supports our conclusion that they represented vertically propagating waves.

In order to evaluate the power and wavelength of these waves, we return to the backscatter observations by the Jicamarca radar. As discussed in paper 1, the strongest vertical radar echoes came from the same region in which the rocket detected these vertically propagating waves. (In fact, it was the radar observations which first led us to consider that the high-frequency in situ observations represented vertical waves.) Since the Jicamarca Doppler spectra show that the mean phase velocities of these waves above 106 km were basically zero (with a significant spread of about ± 75 m/s), we can use this fact to convert the in situ frequencies to wavelengths.

Waves with essentially zero phase velocity appear at in situ frequencies determined by Doppler shifts governed primarily by the vehicle motion. The vertical component of the rocket velocity at 108 km was $+(-)600$ m/s on the upleg (downleg). Thus oscillations at 120 Hz would correspond to 5-m vertical

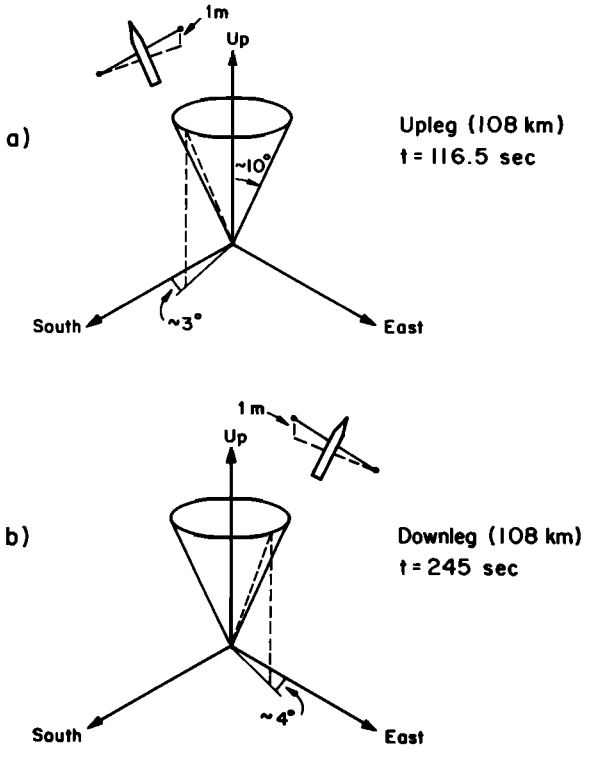

Fig. 6. Position of the payload in its coning cycle during the upleg and downleg traversals of the "pure" two-stream region.

waves, and those at 600 Hz would correspond to 1-m vertical waves. The integrated power profiles in Figures 5*a* and 5*b* were left in terms of measured voltages. If we divide the square root of these powers by the maximum vertical component of the boom, which was about 1 m, we see that the integrated wave amplitudes were roughly 1 mV/m rms on the upleg and 0.4 mV/m rms on the downleg.

The integrated power profiles from 12 to 60 Hz in Figure 5 also corresponded to roughly 1- to 5-m waves for predominantly horizontally propagating waves, assuming a Doppler-shifted rocket frame velocity of 60 m/s, as discussed above. If we divide the square root of these measured values by 5.5 m, we see that the horizontal waves also had integrated amplitudes of the order of roughly 1 mV/m rms. However, the theoretical correction due to the spatial attenuation discussed above would augment the amplitudes of these 1- to 5-m waves measured along the separation distance of 5.5 m by a factor as high as 7 or 8 (although probably somewhat less), whereas the same meter scale waves measured by sensors effectively spaced 1 m apart would not have undergone as significant a spatial attenuation. Thus the horizontally propagating waves were stronger than the vertical ones, although the actual wave amplitudes remain uncertain.

Although undoubtedly oblique waves also contributed to the measured power in each case, the fact that the vertical waves were distinguished at all indicates that they were well organized and stronger than the oblique waves. Because of the fortuitous fact that the predominantly horizontal and vertical waves underwent very different vehicle Doppler shifts, we were able to reliably separate these data into two distinct groups. This result also dramatically demonstrates how waves with the same wavelength but propagating in different directions may simultaneously appear at totally different rocket frame frequencies in a given power spectrum.

Secondary Two-Stream Waves

Introduction. At altitudes below the primary two-stream region (i.e., below 106.5 km) the electron density gradient was unstable. Although the generation of two-stream waves could still take place, now the large-amplitude, horizontally polarized, kilometer scale wave electric fields must be considered in the picture. In this case, the localized plasma drifts are given by $(\mathbf{E} + \delta\mathbf{E}) \times \mathbf{B}$ and may themselves drive either two-stream or gradient drift instabilities [*Sudan et al.*, 1973]. In this section we deal with two-stream waves created by such two-step processes (called "secondary" waves) in the region between roughly 103 and 106.5 km. We refer to this interval as the "interaction" region, since the kilometer scale waves clearly influenced the shorter-scale waves and local instability processes. Thus in this region both the two-stream and gradient drift instabilities were linearly unstable.

Modulation of short-scale waves by the large electric fields. The qualitative relationship of the large-scale horizontal dc electric fields and the higher-frequency (shorter-scale) waves was first shown in Figures 4*a* and 4*b* of paper 2. For example, on the downleg (Figure 4*b*, paper 2), as the large-scale wave electric field turned eastward near 105 km, a large "burst" of higher-frequency waves was observed. More detailed analysis showed that these waves were slightly more pronounced at the edges of the large-scale waveform. On the upleg, as discussed above in regard to Figure 3 of this paper, the topside two-stream waves were cut off abruptly below 106.5 km, where the horizontal perturbation electric field suddenly switched direction from east to west. Another example of this "control" on the upleg occurred at 103 km, where a strong burst of high-frequency waves appeared precisely where the large-scale wave electric field switched eastward. Other examples linking bursts of wave activity with the crests and troughs of large-scale waves can also be seen in the lower electrojet region, as discussed in paper 2.

An expanded view of the relationship between the horizontal dc electric fields and the higher-frequency (shorter-scale) waves is shown in Figure 7 for the interval of 101.5–106.5 km on the upleg. Notice that the relatively high frequency waves occurred in a series of bursts that appeared organized by changes in the dc-coupled electric field, as if they were controlled by the larger structures. Although the actual directions of propagation of the localized bursts of waves are not known (not knowing, for example, the vertical component of the total driving field), some of these waves can be associated with localized $\delta\mathbf{E} \times \mathbf{B}$ plasma flow, as discussed below.

Upgoing and downgoing type 1 waves: A case study. In the lower portion of Figure 7, high-frequency δE spectra are shown for waves detected on the upleg at altitudes of 103 and 105 km. These spectra likely represent two-stream waves because of their high-frequency components and their colocation with strong driving dc electric fields. Notice immediately the difference in the high-frequency characteristics of the electric field spectrum between the two events. At 103 km a sharp break or "knee" occurred at approximately 1000 Hz, whereas at 105 km a similar break occurred near 2000 Hz and displayed more gentle power law slopes. We speculate that the observed characteristics of the spectral break and slopes were influenced by Doppler smearing or compression of an aniso-

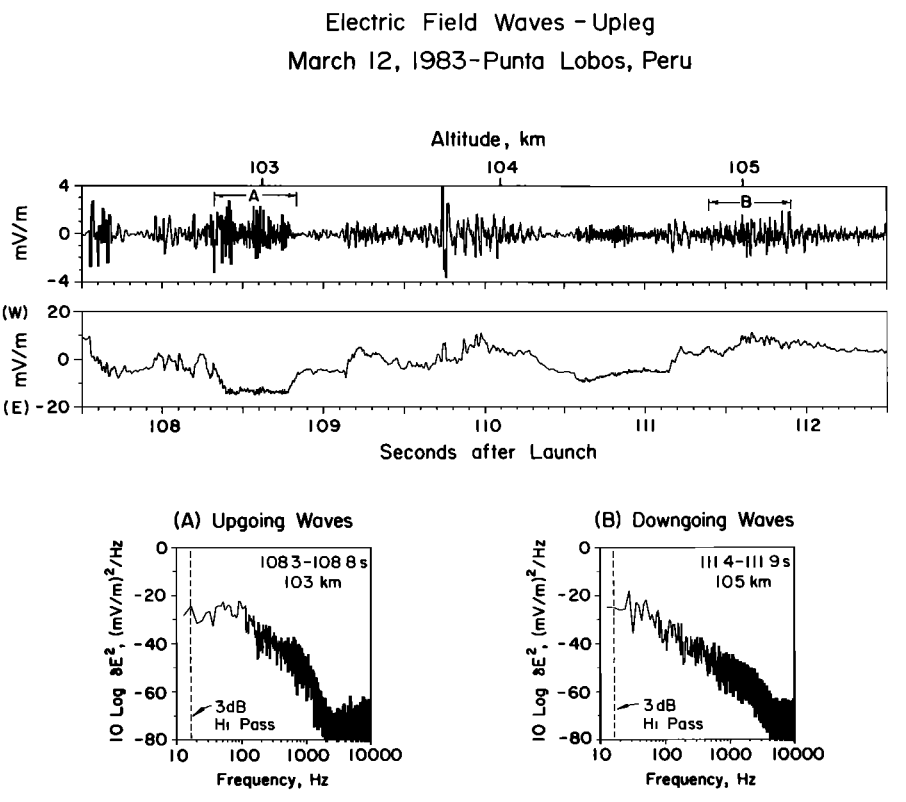

Fig. 7. The upper panels show electric field times series for the upleg indicating the qualitative relationship between the short-scale (high-frequency) waves and the longer-wavelength structures. The lower panels show 0.5-s power spectra of two-stream waves driven by (*a*) eastward and (*b*) westward driving fields. The resulting waves propagated primarily upward and downward, respectively, and underwent very different Doppler shifts imposed by the upgoing rocket motion.

tropic ensemble of unstable waves created by the motion of the upgoing rocket. This can be seen in the following way. The data corresponding to 103 km were embedded in a region of an eastward electric field. Thus assuming a positive vertical component of the vector dc electric field, the unstable two-stream cone was directed in the upward and west quadrant, and the waves were Doppler-shifted to lower rocket frame frequencies since they were propagating along the path of the upgoing vehicle proceeding on a westward azimuth. On the other hand, the waves corresponding to the data at 105 km were embedded in a westward electric field and hence were driven in the downward and west quadrant. In general, these waves were traveling away from the upward rocket velocity direction and hence were Doppler-shifted to higher rocket frame observed frequencies.

An alternative explanation for the different frequencies of the spectral "breaks" between the upgoing and downgoing spectra is that these features mirror changes in the local plasma parameters, such as the ion mean free path or the Debye length. To test these ideas, we examined several other sets of similar spectra, including ones from the downleg near the same altitudes, and found the Doppler shift explanation held in most cases. In one example on the downleg at 105 km, the electric field waves were associated with an eastward field yet were spread out to the highest observed frequencies, similar to the waves detected in the presence of a westward field at the same altitude on the upleg. This is entirely consistent with the Doppler shift explanation, since the downgoing rocket will Doppler-shift the upgoing waves (associated with the eastward electric field) to higher rocket frame frequencies in a symmetrical fashion to the upleg case and the westward field.

In general, given reasonable two-stream phase velocities near the acoustic velocity, the spectral breaks at 1000 Hz and 2000 Hz in these examples corresponded to wavelengths of roughly 50 cm. However, it remains unclear whether this sharp drop was due to the physics of the waves, i.e., due to a real change in the distribution of energy among the unstable wave numbers, or whether it was due to the combined attenuation effect of the boom length factor discussed earlier and the fact that the wavelengths are nearing the finite size of the sensor (4.4 cm diameter), at which point their fields will be shorted out. These same concerns also apply to the observed falloff at high frequencies of the waves in the pure two-stream region (see Figure 1) where the spectral break near 800 Hz would also correspond to scale sizes of tens of centimeters (depending on the propagation direction and Doppler shift). In other words, for very short wavelengths, reliable amplitude measurements are particularly difficult and limit our interpretation of the observed spectral features in this regime.

Summary of the Observations

Below, we summarize the most important results from the in situ electrojet observations of the two-stream waves described above.

1. A strong layer of laminarlike waves was observed by the electric field and plasma density detectors which displayed a peak frequency in the rocket frame near 25 Hz on both the upleg and downleg near 108 km. Since these waves appeared

in the region where the electron current was considered strongest and since the local electron density gradient was stable for growth via the gradient drift instability, this spectral peak is interpreted as being due to a "pure" two-stream process.

2. On the upleg the laminarlike two-stream waves were seen to abruptly "turn on" at a frequency of 72 Hz at 106.5 km altitude, coincident with a change in the east-west horizontal electric field. The waves slowly shifted to a lower rocket frame frequency with increasing altitude. This change in frequency may be explained by the fact that the waves were traveling faster at the higher altitudes and were subsequently shifted to lower rocket frame frequencies by the vehicle Doppler shift.

3. The primary two-stream waves were polarized primarily in the east-west direction along the magnetic equator and had wavelengths that were generally less than 10 m. The primary wavelengths appeared to peak between roughly 2 and 3 m.

4. The observations suggest that if the phase velocity of the primary two-stream waves on the upleg was near 380 m/s when the waves "turned on" at 106.5 km, the phase velocity then increased to roughly 500 m/s at 108 km, provided the peak wavelength in the plasma reference frame remained about the same.

5. The measured electric field amplitude of the primary two-stream waves was roughly 2 mV/m rms with density fluctuations of 1–2% rms. The electric field amplitude, given the expected attenuation imposed by the finite boom length effect, may have been several times larger than this value.

6. A distinct component of meter scale waves propagating perpendicular to the current (vertically) was also observed in the region of the "pure" two-stream waves and had associated electric fields of roughly 1 mV/m rms. These waves appear to have been the same as those responsible for the scattering of the Jicamarca vertical radar signal in the upper two-stream region.

7. The large-amplitude gradient drift driven waves below 106 km clearly influenced the short-scale waves which appeared in groups of bursts organized by the kilometer scale electric field structures.

8. Spectra corresponding to two-stream waves driven by upward and downward directed plasma drifts showed a marked difference in the rocket frame, which can be interpreted as resulting from drastically different Doppler shifts imposed by the moving probe.

9. The high-frequency portion of the electric field two-stream spectra indicated that wavelengths were detected with scale sizes at least as short as 50 cm.

3. DISCUSSION

Primary Two-Stream Region

Phase velocity. For over two decades, VHF and HF backscatter radar observations of vertical and oblique type 1 (two-stream) echoes have shown that the phase velocities of the two-stream waves in the equatorial electrojet are limited to a value near the acoustic velocity (see review by *Fejer and Kelley* [1980]). Several theories have been proposed which suggest various nonlinear velocity saturation mechanisms which might explain this observed phenomenon [see *Sudan*, 1983*a*, and references therein]. The radar data further indicate that the magnitude of the phase velocity is invariant with respect to zenith angle within the two unstable quadrants containing the positive direction of the current.

The in situ evidence presented in this paper suggests that the phase velocities of the topside horizontal two-stream waves at 108 km where the current is believed to be strongest did not appear to be limited but, instead, had values ($\sim$500 m/s) nearer to those predicted by linear theory. To make this comparison, we estimate the linear phase velocity of the two-stream waves predicted by $V_\phi = V_d \cos\theta/(1 + \psi)$ for propagation parallel to the current to be 485 m/s, in which we have used a value of 0.06 for ψ (the ratio of the electron and ion collision frequencies to their gyro frequencies) and have taken the drift velocity V_d from the calculations in paper 2 for 108 km. The very fact that the waves appeared to "switch on" and then smoothly change frequency (interpreted as speeding up) lends further support that they were governed by a changing plasma drift velocity. The absence of this same observed frequency change on the downleg can be accounted for by the fact that the rocket probes encountered a different phase of the large-scale waves at their interface with the laminar two-stream layer and hence the polarization field (and thus the plasma drift) was modulated in a different fashion.

At first glance, the correspondence of the phase velocities estimated from the rocket data and those predicted by linear theory appears to contradict the long-standing backscatter radar results. However, since these primary two-stream waves were horizontally polarized, their backscattered echoes could only be observed by VHF radar beams directly horizontally. (Note that the steerable radar at Jicamarca can receive echoes from up to 60° from the vertical.) Indeed, *Lee et al.* [1974] point out that a region of two-stream waves may very well exist in the upper portion of the daytime electrojet which would not be observable by VHF backscatter radars, consistent with our interpretation. Furthermore, primary waves near the skirts of the unstable cone would propagate slower than the horizontal waves by a $\cos\theta$ factor and thus would contribute radar Doppler velocities near C_s in the steerable radar data. On the other hand, HF radars, which typically measure irregularities with scale sizes of roughly 10 m, can sometimes take advantage of radio wave refraction to observe horizontally propagating waves [*Crochet et al.*, 1979] but measure irregularities with longer scale sizes. Such systems typically have broad beam widths, however, which may preclude a definitive resolution of the thin laminarlike layer that we have observed in this experiment.

On the basis of the data reported here, the type 1 echoes received by the very broad beam antennas, such as the steerable VHF system at Jicamarca or the portable HF system at Ancon, whose beams were oriented obliquely into the scattering layer, probably originated from oblique secondary two-stream waves driven by the large-scale waves below the "pure" laminar two-stream layer. In the region between 103 and 106 km, where the large-scale wave interaction was strongest, the secondary two-stream scattering packets would be expected to dominate the oblique k directions filling the broad-beam radars. Note that these radar backscatter spectra would yield phase velocities that are governed by $(\delta\mathbf{V}_d + \mathbf{V}_d)/(1 + \psi)$ plus a neutral wind component and that ψ may be between 0.2 and 0.3 in this region, much larger than at 108 km. The phase velocities of the oblique and vertical secondary two-stream waves in the upper large-scale turbulent region ($\sim$105 km) may indeed have been limited at a velocity near the acoustic speed, although it is unclear whether the secondary waves themselves were limited by some process intrinsic to the short-wavelength regime or whether (as an alternative explanation) the electric field amplitudes of the driving, large-scale waves

were themselves limited at values such that $\delta E/B(1 + \psi) \sim C_s$. We will address the phase velocities of the secondary waves in detail later on in this section. For now, we continue the discussion of the primary two-stream oscillations.

The existence of a laminarlike layer in the equatorial electrojet was actually first discussed in a series of papers dealing with observations during the counterelectrojet in the daytime [*Crochet et al.*, 1979; *Hanuise and Crochet*, 1981; *Crochet*, 1981]. In the counterelectrojet experiment, since the direction of the electron drift changed sign, the normally unstable upward density gradient in daytime conditions was stable. These authors claim that in this case, a laminar two-stream region developed, devoid of strong contributions from the gradient drift instability. The HF radar observations [*Crochet et al.*, 1979] showed that the phase velocities of the oblique two-stream waves varied over several hours in accordance with changes in the electron drift velocity (inferred from the ground-based magnetometer and a model density profile). These measurements were interpreted in terms of the linear theory and were used to distinguish between laminar and turbulent conditions. The data presented here indicate that a laminar layer "resided" on the top of the large-scale turbulence even during "typical" daytime conditions. Therefore we propose that this may indeed be a common situation, provided that the electron current is strong enough to produce primary two-stream waves and the local electron density gradient is stable.

Despite the fact that the in situ observations indicate that the horizontally propagating coherent waves were traveling in the direction of the current and possibly near the $\mathbf{V}_d/(1 + \psi)$ velocity, there remain a number of open questions in our analysis which suggest that the conclusion that the phase velocity of the waves "obeyed" linear theory may not be so certain.

First, why do the waves not appear to slow down on the very top part of the layer where presumably the current density must weaken? Even if the slope in the current density was very sharp, it is surprising that there was no indication at all of this effect. A change in the neutral wind velocity in this region could have masked the change in the wave phase velocity, although it is doubtful that the two velocities would cancel each other so conveniently. Perhaps the nonlinear effects which account for the generation of the meter scale vertical waves embedded in the laminar layer (discussed later on) and which appeared most pronounced in both the radar and rocket data on the very topside, are important factors in controlling the phase velocity of the primary two-stream waves. Clearly, we do not understand the lack of an observed decrease in the horizontal phase velocity on the very topside of the two-stream layer.

Second, the local electron temperature may have been elevated in the upper portion of the layer, possibly because of the effects of the waves themselves. The theory of heating by electrojet waves has been developed in several papers [e.g., *St.-Maurice et al.*, 1981; *St.-Maurice and Schlegel*, 1983; *St.-Maurice and Laher*, 1985; *St.-Maurice et al.*, 1986]. In this case, however, in order for the acoustic velocity to have increased from 380 m/s to 500 m/s, the electron temperature would have required an increase from 260° to 454° in the narrow altitude range of 2 km, which is unlikely. Also, this would not explain the absence of a similar observed variation on the downleg.

Before leaving this point, however, we remark that if the waves did propagate at a controlled "threshold" acoustic velocity (but perhaps an elevated one), then this would be at least consistent with the lack of a decrease in the observed phase velocity at the very top part of the two-stream region, even if the electron drift velocity had slowed at this point.

Spectrum. Although the fluid theory is useful for determining the onset of the two-stream instability, since the majority of two-stream wavelengths are a few meters and shorter, kinetic theory is needed to evaluate the amplitudes of the unstable wave numbers. The collisional two-stream kinetic theory was first developed by *Farley* [1963]. *Schmidt and Gary* [1973] extended this work by including the effects of density gradients for conditions of the daytime equatorial electrojet. Other researchers [e.g., *Lee et al.*, 1971; *Ossakow et al.*, 1975] have published similar treatments including the effects of strong electron drifts (several times the acoustic velocity) and parallel propagation.

Basically, the kinetic treatment for the two-stream instability shows that near marginal instability the growth rate peaks at wavelengths of a few meters. The lower panel of Figure 8 shows the growth rate computed by *Schmidt and Gary* [1973] in the absence of density gradients. The conditions for this computation corresponded to daytime equatorial electrojet parameters which were very similar to the ones present in our experiment. The drift velocity (500 m/s) and electron temperature (230°) used by these authors were such that $V_d/C_s = 1.4$.

The in situ measured spectrum of the two-stream waves observed at 108 km altitude is also plotted in Figure 8. The

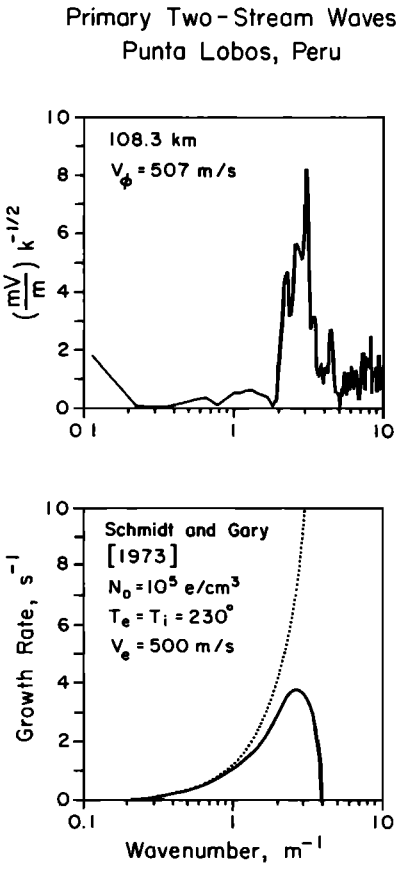

Fig. 8. Comparisons of the measured electric field wave spectrum and two-stream growth rate calculations by *Schmidt and Gary* [1973] for daytime equatorial conditions. The dotted line in the growth rate calculation is the result of the fluid theory, and the solid line represents the kinetic results.

frequencies have been converted to wave numbers by assuming propagation along the magnetic equator at 506 m/s. The amplitudes have been corrected for the spatial attenuation specified by equation (2), as discussed earlier.

Notice the overall agreement between the wave number domain of the measured waves with that which the growth rate indicates will be unstable. In particular, notice that the peak in the measured power at roughly $k = 2.8$ m^{-1} agrees nicely with the growth rate peak at $k = 2.6$ m^{-1}. A similar spectrum was also observed in the $\delta n/n$ data (see Figure 4) which supports our interpretation of the observed oscillations as electrostatic two-stream plasma waves. The agreement between the observed principal wavelengths of the two-stream waves and the growth rate implies that the peak in the growth rate (i.e., where the waves grow the fastest at the onset) is also where the majority of the wave energy remains, in contrast to the gradient drift case, where the largest amplitudes were observed at wavelengths considerably longer than those of the most unstable linear modes, as shown in paper 2.

As discussed in regard to the fluid growth rate computations in paper 2, although there will be a small positive contribution to two-stream growth at long wavelengths, in this case, damping by the gradient drift and recombination terms produce a long-wavelength cutoff. The measured spectrum shows a significant rise corresponding to a wavelength of approximately 6 m which is somewhat sharper than the gradual rise shown in the growth curve in Figure 8. The smaller wave numbers were difficult to measure in this experiment because of the strong vehicle Doppler shift. In general, however, the low unstable wave number domain predicted theoretically is in good agreement with the measurements.

At the shortest scales (highest k values), several important physical properties come into effect to limit growth, such as ion Landau damping [e.g., *Lee et al.*, 1971; *Schmidt and Gary*, 1973]. Although the growth curve in Figure 8 shows a sharp upper cutoff at 1.6 m, other kinetic theory studies indicate that growth may be pushed to scale sizes of the order of tens of centimeters and is strongly dependent on the strength of the driving current [e.g., *Lee et al.*, 1971]. In the case where the primary two-stream waves are continuously generated, nonlinear wave interactions probably produce some small net power at very short wavelengths. Although these modes may be damped, they would be replaced by new ones provided the instability mechanism was not shut off.

The higher-frequency part of the observed two-stream spectrum (see Figure 1) is not easy to interpret. The observed high-frequency waves contained contributions from vertical, oblique, and horizontal wave numbers corresponding to scales at least as small as 0.5 m wavelength, as inferred directly from the data. The actual spectral estimates of these wave numbers, however, are uncertain, for the reasons discussed earlier. Thus we refrain from interpreting the measured high-frequency rolloff or "knee" in terms of physical parameters such as the electron gyroradius (about 2 cm) or the ion mean free path (about 15 cm), since both the conversion from frequency to wave number and the wave amplitudes are ambiguous for such short scales.

Relationship of δE and $\delta n/n$. The observed relationship between δE and $\delta n/n$ for the primary two-stream waves provides additional insight into the nature of the instability and into the validity of our interpretation. The relationship between δE and $\delta n/n$ can be derived directly from first-order perturbation analysis of the combined electron and ion continuity and momentum fluid equations [e.g., *Fejer*, 1984]. In this case, for wavelengths smaller than a few hundred meters we have

$$\frac{\delta E}{E} = \left[\frac{\nu_i}{\Omega_i}\frac{1}{(1+\psi)} - \frac{ikC_s^2}{2\Omega_i V_d}\right]\frac{\delta n}{n} \tag{3}$$

where we have assumed $T_e = T_i$ and the variables are defined as before.

For $k = 2.5$ m^{-1}, the value of the first term in (3) is roughly 22.5 while the second is -3.9, yielding an amplitude ratio of $\delta E/E$ to $\delta n/n$ of 23 and a phase difference of about 10° with δn leading δE. From the analysis of the data in Figure 4 the integrated rms amplitudes of δE and $\delta n/n$, for k values from 1.7 to 5.4 m^{-1}, yielded 7.3 mV/m and 1.1%, respectively. For a 13.5-mV/m polarization field the experimental ratio of $\delta E/E$ to $\delta n/n$ would be roughly 50. This ratio is therefore higher by a factor of 2 than that expected from (3). The most probable source of the amplitude discrepancy lies in an overestimate of the electric field wave amplitudes for the reasons discussed in the data presentation section. Note that if no spatial attenuation correction factor had been used, the $\delta E/E$ to $\delta n/n$ ratio would have been only 6.5, far below that predicted by (3). Nonlinear alterations of (3) may also be important.

Vertically propagating waves in the "pure" two-stream layer. So far in this section, we have been discussing the observations of the horizontally propagating two-stream waves in the laminar layer on the topside of the electrojet. But this is not the whole story of the fully developed two-stream spectrum. A strong component of meter scale vertically oriented waves was also observed in this region, which we interpret as part of the fully evolved, steady state two-dimensional two-stream spectrum.

The in situ observations of vertical meter scale turbulence associated with the horizontal two-stream waves have been interpreted in conjunction with the radar data reported in paper 1, where it was shown that the most appealing mechanism to explain the vertical waves involves some sort of mode-mode coupling, such as the three-wave interaction process [e.g., *Kraichnan*, 1959; *Kadomtsev*, 1965; *Dougherty and Farley*, 1967]. In general, these ideas permit any two wave vectors to give rise to a third, provided the resonant interaction conserves both wave energy and momentum. For two nearly parallel wave vectors with nearly equal magnitudes (such as are present in the primary two-stream instability cone), the resulting coupled vector will arise nearly perpendicular to these waves (in this case, vertical) with a near-zero phase velocity, in agreement with the observations. The coupled modes may then interact with other coupled modes as well as with other primary "parent" modes.

At first glance it appears that the resulting picture would ultimately produce an isotropic distribution of turbulent wave fields. The in situ observations show, however, that the wave electric fields were not isotropically distributed but rather were more pronounced in the vertical and horizontal directions. It seems intuitively sound, however, that as long as energy is continually being pumped into a narrow cone of horizontal, primary wave numbers, then the final, steady state spectrum will not be isotropic but will maximize in both the horizontal and vertical directions, with some lesser degree of oblique wave power also being generated. The fact that the vertical wave vectors observed in situ appeared more distinct on the very topside (109–111 km) of the two-stream layer suggests that possibly the oblique wave vectors may have been

stronger at slightly lower altitudes and then tapered off at higher altitudes. Indeed, as the drift velocity weakens and approaches C_s on the very topside, the unstable primary cone becomes very narrow and would effectively limit the production of obliquely coupled modes. Note that because these mode coupled waves do not produce type 1 backscatter radar signatures, the in situ observation that the vertical waves appeared stronger than the oblique ones on the topside does not contradict the result of *Ierkic et al.* [1980] that the minimum cross section of type 1 waves is in the vertical direction.

The narrowing cone on the very topside would suggest that somewhat longer vertical wavelengths might be expected to be observed by in situ probes at slightly higher altitudes than the upper limit of where the radar detected vertical 3-m echoes. In this experiment, however, just the opposite was observed. The radar detected very strong 3-m vertical waves that were abruptly cut off a kilometer or two higher than the uppermost limit of the high-frequency oscillations detected in situ. The actual height discrepancy may not be significant and possibly can be explained by the fact that the radar was more sensitive than the electric field detector or that the rocket and radar did not sample a common volume. Nevertheless, the absence of any oscillations in the rocket data above the maximum height where the radar detected these waves suggests that the vertical spectrum was sharply limited to short-scale waves, confirms that these waves did not significantly propagate away from their source, and implies that they were associated with an instability process with a well-defined threshold.

Secondary Two-Stream Waves

The existence of 3-m two-stream (type 1) backscatter radar echoes in the vertical direction indicates that such waves must propagate outside of the unstable cone centered in the horizontal direction associated with the main electrojet current. *Sudan et al.* [1973] postulated that such waves can be generated via a two-step process, in which the plasma drift associated with large horizontal electric fields would generate "secondary" waves propagating in both the vertical (upward or downward) and oblique directions.

The criterion for the generation of secondary two-stream waves is given by

$$\delta E/B \geq C_s(1 + \psi) \tag{4}$$

where δE is the wave electric field, perpendicular to the magnetic field and to the center of the resulting cone of unstable wave vectors. Thus, given reasonable values of the acoustic velocity and ψ at the magnetic equator in Peru, the wave fields must be of the order of 10–15 mV/m in order to generate vertical secondary two-stream waves near 105 km altitude. The rocket-measured wave electric fields on the upleg and downleg were of this order, and thus this result confirms the ideas of *Sudan et al.* [1973] in regard to how vertical secondary two-stream waves can be generated.

Notice in paper 1 that the VHF vertical type 1 (i.e., two-stream) echoes were seen only in the narrow altitude range of 102–106 km, whereas the in situ observations of the large-scale wave electric fields had amplitudes from 10 to 15 mV/m throughout a much wider altitude range, from roughly 92 to 106 km. This discrepancy can easily be explained by the fact that at the lower altitudes the ψ term becomes large (see Figure 5*a*, paper 2), and thus secondary two-stream waves were not generated via (4), despite the fact that the electric field amplitudes remained more or less large throughout the layer.

To illustrate this point, the $\delta\mathbf{E} \times \mathbf{B}$ velocities associated with the measured wave electric fields are plotted versus altitude in Figure 9. Because the third electric field component was not included in the analysis and the spin plane components departed from the horizontal plane by 10°, these measured horizontal fields could be off by as much as ± 1–3 mV/m, particularly in the region of the strong electrojet current, because of contributions from the unknown polarization field. In principle, this source of error could change the measured vertical velocities by roughly 100 m/s in either direction. A dotted line indicates the approximate values of $\pm C_s(1 + \psi)$, using a constant value for C_s of 380 m/s. In reality, C_s decreases with lower altitude, although it falls off much more slowly than ψ in this region and increases with higher altitude. The region where the velocities were approximately equal to this value corresponded to where the Jicamarca radar observed vertical type 1 echoes.

Despite the conclusion that the measured in situ wave fields were large enough to generate vertically propagating secondary two-stream waves, notice that the amplitudes of the driving fields were actually not that much larger than $C_s(1 + \psi)$. Other reported horizontal electric fields in the equatorial electrojet [*Sartiel*, 1977; *Prakash and Pal*, 1985] showed similar amplitudes, but not larger than what we have measured here. Thus the vertical phase velocities which corresponded to $\delta E/[B(1 + \psi)]$ would not have been much larger than the type 1 velocities that were observed by the VHF radar at Jicamarca and that are claimed to "saturate" at the acoustic velocity. The evidence for the saturation of the type 1 waves observed at Jicamarca is seen in the flat-topped nature of their Doppler spectra, which also serve as tracers of the large-scale waves. However, it is not clear by looking at the radar data whether the secondary phase velocities were braked at the

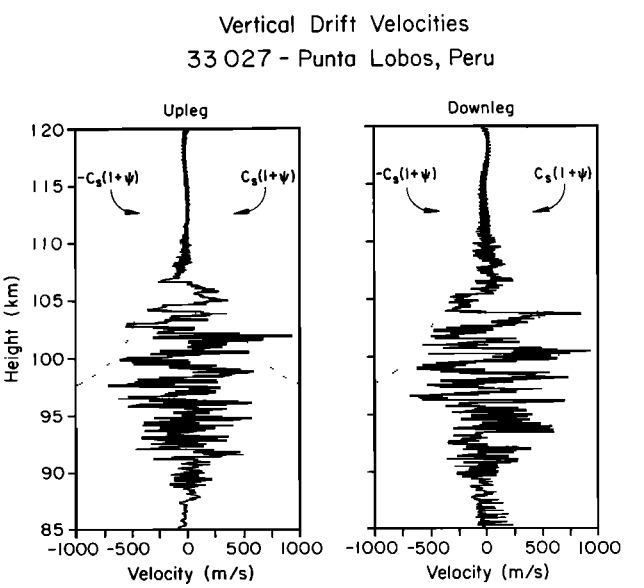

Fig. 9. Vertical drift velocities associated with the horizontal electric fields measured during the upleg and downleg traversals of the electrojet. The boundaries corresponding to $\pm C_s(1 + \psi)$ which represent the two-stream instability threshold are also shown for a fixed value of T_e. The measured drift velocities may be off by roughly ± 100 m/s, as explained in the text.

threshold (acoustic) speed or whether the driving large-scale wave electric fields were limited instead.

To address this point, we consider the shape of several of the large horizontal wave electric fields measured in situ in the region where the electrojet current was strong. As shown in Figure 10, notice that these fields were "flat-topped," exhibiting a squarelike shape. Thus, without regard to an additional saturation mechanism, the secondary two-stream phase velocities driven by the electric fields of these waves would also show a flat-topped signature, similar to the observed Jicamarca vertical type 1 spectra. These observations suggest that the phase velocities of type 1 secondary waves may be limited because of the saturation of the driving electric fields rather than a process intrinsic to the two-stream process itself. In addition, the sharp edges of the in situ measured electric field waveforms are consistent with the rapid reversals between upgoing and downgoing type 1 waves observed at Jicamarca. We argue here that the pattern traced out by the vertical two-stream radar echoes at Jicamarca is actually that of the large-scale horizontal driving electric fields.

The appearance of limited phase velocities from steerable backscatter radars may also be primarily a consequence of the saturated horizontal electric fields. In this case, for echoes originating in the region of the large-scale waves, if both the polarization field and the east-west electric fields are limited by the nonlinear interaction of the large-scale waves and the electrojet current [*Kudeki et al.*, 1985], obliquely propagating wave phase velocities would also appear limited at a value not far from $2^{1/2}C_s$ (for 45° and $E/B \sim \delta E/B \sim C_s$). Although some variation would then be expected with respect to zenith angle, this may fall within the experimental error, particularly since the neutral wind contribution already substantially alters the

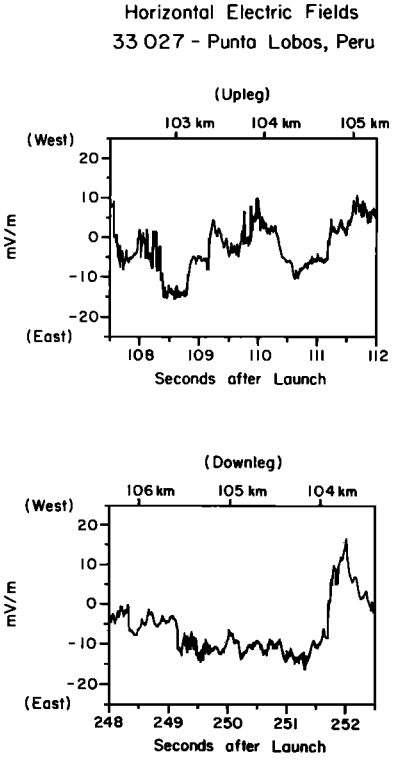

Fig. 10. Enlarged representations of the horizontal large-scale electric fields showing the steepened, flat-topped waveforms observed in the region of strong electrojet current for both the upleg and the downleg.

Doppler shift (and hence the inferred phase velocity) of the oblique echoes. Note also that the steerable antennas at the equator have large beam widths and may typically integrate echoes received over the space of several large-scale wavelengths. Furthermore, as noted earlier, since these steerable VHF radars do not receive echoes originating from waves propagating in the horizontal direction, any contributions to the steerable data from the topside, primary two-stream waves would be from waves generated near the skirts of the horizontal unstable cone and hence would also be near C_s.

At first glance, using the saturated electric fields to explain the limited type 1 phase velocities suggests that the neutral wind derivations from backscatter Doppler spectra based on the constant velocity assumption [*Balsley et al.*, 1976] may have to be modified. However, because $\delta E \sim E$ and because the observed values of $\delta E/B(1 + \psi)$ are very close to C_s anyway, the adjustment would not necessarily be significant. In fact, the estimate of the neutral wind in this experiment relied on the assumption that the Jicamarca vertical and oblique phase velocities were equal, and we showed evidence in paper 2 that this estimate was consistent with an inference of the neutral wind velocity from the observed large-scale wave phase velocity.

Finally, in support of our hypothesis that the type 1 phase velocities are governed by the local drift velocities and are chiefly responding to the nonlinearly saturated amplitudes of the large-scale wave electric fields, we note that several laboratory experiments have shown that two-stream wave phase velocities do not saturate at the acoustic velocity but rather appear to correspond more closely to the linear theory result [*D'Angelo et al.*, 1974; *John and Saxena*, 1975], as we suggest.

The amplitudes of the observed large-scale waves and their nonsinusoidal shapes present a fresh look at the puzzling observation of the saturation of type 1 secondary phase velocities. The ideas put forth here do not preclude the existence of other two-stream phase velocity saturation mechanisms or of a combination of competing mechanisms. Indeed, several characteristics of the primary, horizontal two-stream wave phase velocities on the topside discussed earlier appear more puzzling than those of the secondary, vertical two-stream waves. We speculate that the detailed physics that determines the steady state phase velocities of the horizontally propagating primary two-stream waves embedded in a continuous, laminarlike layer of meter scale turbulence, such as in the topside of the equatorial electrojet at 108 km or in the auroral zone electrojet, may be different from that governing the velocities of the upgoing and downgoing two-stream waves which turn on and off very rapidly, like a switch. In the case of oscillating packets of vertically oriented secondary two-stream waves, if a phase velocity saturation mechanism intrinsic to the waves were to exist [e.g., *Sudan*, 1983*a*], the medium must organize very fast (i.e., the time constant of the saturation mechanism must be exceedingly short) to "brake" the waves at their onset, since the observed radar phase velocities appear limited immediately as the waves turn on. This situation is easily explained if the phase velocities are governed instead by the saturated driving fields.

4. Conclusions

In this paper we have carried out a detailed investigation of in situ observations of both primary and secondary two-stream waves in the equatorial electrojet over Peru. The main conclusions of our analysis are as follows:

Primary Two-Stream Waves

1. Coherent, narrowly banded oscillations observed simultaneously by in situ δE and $\delta n/n$ detectors at 108 km represent horizontally propagating primary waves produced by the collisional two-stream instability.

2. The horizontal waves were most distinct in a narrow altitude range of 2 km centered at 108 km where the current was believed to have been strongest, which is consistent with the generation of these waves by a current-driven instability.

3. The measured peak wavelength of 2–3 m shows excellent agreement with the wavelength of the most unstable modes (peak growth rates) calculated from kinetic theory for similar plasma parameters in the daytime equatorial electrojet.

4. The phase velocity of the primary two-stream waves showed evidence of being controlled by changes in the local plasma drift velocity and may have been comparable to the linear theory result.

5. Because the primary two-stream waves propagate horizontally along the direction of the current, VHF backscatter radars looking vertically or obliquely would not be expected to observe these waves, as predicted by *Lee et al.* [1974]. The constant phase velocities observed by the radars are not in contradiction with the horizontal phase velocities observed in situ, since the oblique and vertical two-stream waves observed by backscatter radars at the equator could originate primarily in the interaction region of large-scale waves and not from the laminar topside layer.

6. The phase velocity of the horizontally propagating waves did not appear to decrease on the very topside, where presumably the current density must weaken. This remains puzzling and suggests that there remain several aspects of the topside two-stream waves that are not yet understood.

7. The strong component of vertical waves associated with the "pure" two-stream region observed by both the Jicamarca radar and the in situ electric field instruments may possibly be explained by a mode-mode coupling process, as discussed in paper 1. The vertically propagating waves which appeared most well organized on the very topside of the layer may be a consequence of the fact that the primary instability cone is narrowest near marginal instability.

Secondary Two-Stream Waves

1. The amplitudes of the observed large-scale horizontal electric fields (10–15 mV/m) were large enough to generate vertical secondary two-stream waves via a two-step process as proposed by *Sudan et al.* [1973].

2. The fact that ψ becomes large below 102 km explains why both the rocket probes and the Jicamarca radar only observed secondary two-stream waves between 102 and 106 km, despite the fact that the observed kilometer scale wave electric field amplitudes remained large ($\sim$10–15 mV/m) below 102 km.

3. The observation that the steepened waveforms of the large-scale, east-west electric fields abruptly changed directions in the central region of the electrojet explains the observations by the Jicamarca radar of a rapid switching between upgoing and downgoing two-stream (type 1) radar echoes.

4. The flat-topped amplitudes of the large-scale waves imply that the phase velocities of the secondary vertical waves they generate will also be limited. This suggests that the appearance of saturated type 1 phase velocities in backscatter coherent radar spectra may be due primarily to a limitation of the driving electric fields rather than due to a process intrinsic to the two-stream mechanism itself.

Acknowledgments. We acknowledge useful discussions with D. T. Farley. We thank the staff of Jicamarca Observatory for providing the radar observations. Project Condor was a joint undertaking of the National Aeronautics and Space Administration (NASA) of the United States and of the Instituto Geofisico del Peru (IGP) and the Comision Nacional de Investigacions y Desarrollo Aerospacial (CONIDA) of Peru. We thank all of the personnel involved in the launch operations for their support and expertise in carrying out this experiment, and in particular, we acknowledge David Detwiler, the rocket payload manager at NASA/Wallops Flight Facility. The work at Cornell ws sponsored by NASA under grant NSG-6020 and by the Division of Atmospheric Sciences of the National Science Foundation through grants ATM-8218619, ATM-8305500, and ATM-8418717.

The Editor thanks P. K. Chaturvedi and R. A. Greenwald for their assistance in evaluating this paper.

REFERENCES

Bahnsen, A., E. Ungstrup, C.-G. Falthammar, U. Fahleson, J. K. Olesen, F. Primdahl, F. Spangslev, and A. Pedersen, Electrostatic waves observed in an unstable polar cap ionosphere, *J. Geophys. Res.*, *83*, 5191, 1978.

Baker, K. D., J. LaBelle, R. F. Pfaff, L. C. Howlett, N. B. Rao, J. C. Ulwick, and M. C. Kelley, Absolute electron density measurements in the equatorial ionosphere, *J. Atmos. Terr. Phys.*, *47*, 781, 1985.

Balsley, B. B., B. G. Fejer, and D. T. Farley, Radar measurements of neutral winds and temperatures in the equatorial *E* region, *J. Geophys. Res.*, *81*, 1457, 1976.

Buneman, O., Excitation of field aligned sound waves by electron streams, *Phys. Rev. Lett.*, *10*, 285, 1963.

Crochet, M., Review of the equatorial electrojet instability in light of recent developments in HF radar measurements, *J. Atmos. Terr. Phys.*, *43*, 579, 1981.

Crochet, M., C. Hanuise, and P. Broche, HF radar studies of two-stream instability during an equatorial counterelectrojet, *J. Geophys. Res.*, *84*, 5223, 1979.

D'Angelo, N., H. L. Pecseli, and P. I. Petersen, The Farley instability: A laboratory test, *J. Geophys. Res.*, *79*, 4747, 1974.

Dougherty, J. P., and D. T. Farley, Ionospheric *E* region irregularities produced by nonlinear coupling of unstable plasma waves, *J. Geophys. Res.*, *72*, 895, 1967.

Dupree, T. H., A perturbation theory for strong plasma turbulence, *Phys. Fuids*, *9*, 1773, 1966.

Farley, D. T., A plasma instability resulting in field-aligned irregularities in the ionosphere, *J. Geophys. Res.*, *68*, 6083, 1963.

Farley, D. T., Theory of equatorial electrojet plasma waves: New developments and current status, *J. Atmos. Terr. Phys.*, *47*, 729, 1985.

Fejer, B. G., Small scale plasma irregularities in the auroral lower ionosphere, *Phys. Space Plasmas*, *5*, 73, 1984.

Fejer, B. G., and M. C. Kelley, Ionospheric irregularities, *Rev. Geophys.*, *18*, 401, 1980.

Hanuise, C., and M. Crochet, 5- to 50-m wavelength plasma instabilities in the equatorial electrojet, 3, Counterelectrojet conditions, *J. Geophys. Res.*, *86*, 7761, 1981.

Ierkic, H. M., B. G. Fejer, and D. T. Farley, The dependence on zenith angles of the strength of 3-m equatorial electrojet irregularities, *Geophys. Res. Lett.*, *7*, 497, 1980.

John, P. I., and Y. C. Saxena, Observation of the Farley-Buneman instability in laboratory plasma, *Geophys. Res. Lett.*, *2*, 251, 1975.

Kadomtsev, B. B., *Plasma Turbulence*, Academic, Orlando, Fla., 1965.

Kelley, M. C., and F. S. Mozer, Electric field and plasma density oscillations due to the high-frequency Hall current two-stream instability in the auroral *E* region, *J. Geophys. Res.*, *78*, 2214, 1973.

Kintner, P. M., J. LaBelle, M. C. Kelley, L. J. Cahill, Jr., T. Moore, and R. Arnoldy, Interferometric phase velocity measurements, *Geophys. Res. Lett.*, *11*, 19, 1984.

Kraichnan, R. H., The structure of isotropic turbulence at very high Reynolds numbers, *J. Fluid Mech.*, *5*, 497, 1959.

Kudeki, E., D. T. Farley, and B. G. Fejer, Theory of spectral asymmetries and nonlinear currents in the equatorial electrojet, *J. Geophys. Res.*, *90*, 429, 1985.

Kudeki, E., B. G. Fejer, D. T. Farley, and C. Hanuise, The Condor

equatorial electrojet campaign: Radar results, *J. Geophys. Res.*, this issue.

Lee, K., and C. F. Kennel, Effects of propagation parallel to the magnetic field on the type 1 electrojet irregularity instability, *Planet. Space Sci.*, *21*, 1339, 1973.

Lee, K., C. F. Kennel, and J. M. Kindel, High frequency Hall current instability, *Radio Sci.*, *6*, 209, 1971.

Lee, K., C. F. Kennel, and F. V. Coroniti, On the marginally stable saturation spectrum of unstable type 1 equatorial electrojet irregularities, *J. Geophys. Res.*, *79*, 249, 1974.

Ossakow, S. L., K. Papadopoulos, J. Orens, and T. Coffey, Parallel propagation effects on the type 1 electrojet instability, *J. Geophys. Res.*, *80*, 141, 1975.

Pfaff, R. F., Rocket studies of plasma turbulence in the equatorial and auroral electrojets, Ph.D. thesis, Cornell Univ., Ithaca, N.Y., 1986.

Pfaff, R. F., M. C. Kelley, B. G. Fejer, E. Kudeki, C. W. Carlson, A. Pedersen, and B. Häusler, Electric field and plasma density measurements in the auroral electrojet, *J. Geophys. Res.*, *89*, 236, 1984.

Pfaff, R. F., M. C. Kelley, B. G. Fejer, N. C. Maynard, L. H. Brace, B. G. Ledley, L. G. Smith, and R. F. Woodman, Comparative in-situ studies of the unstable day-time equatorial *E*-region, *J. Atmos. Terr. Phys.*, *47*, 791, 1985.

Pfaff, R. F., M. C. Kelley, E. Kudeki, B. G. Fejer, and K. D. Baker, Electric field and plasma density measurements in the strongly driven daytime equatorial electrojet, 1, The unstable layer and gradient drift waves, *J. Geophys. Res.*, this issue.

Prakash, S., and S. Pal, Electric fields and electron density irregularities in the equatorial electrojet, *J. Atmos. Terr. Phys.*, *47*, 853, 1985.

Prakash, S., S. P. Gupta, B. H. Subbaraya, and C. L. Jain, Electrostatic plasma instabilities in the equatorial electrojet, *Nature*, *233*, 56, 1971.

Prakash, S., B. H. Subbaraya, and S. P. Gupta, Rocket measurements of ionization irregularities in the equatorial ionosphere at Thumba and identification of plasma irregularities, *Indian J. Radio Space Phys.*, *1*, 72, 1972.

Rogister, A., Nonlinear theory of type 1 irregularities in the equatorial electrojet, *J. Geophys. Res.*, *76*, 7754, 1971.

Rogister, A., and N. D.'Angelo, Type 2 irregularities in the equatorial electrojet, *J. Geophys. Res.*, *75*, 3819, 1970.

Sartiel, J., Champs électriques dans la région de l'électrojet équatorial, Ph.D. thesis, Univ. of Paris, VI, 1977.

Sato, T., Stabilization of the two-stream instability in the ionosphere, *Phys. Rev. Lett.*, *28*, 732, 1972.

Schmidt, M. J., and S. P. Gary, Density gradients and the Farley-Buneman instability, *J. Geophys. Res.*, *78*, 8261, 1973.

Sleeper, A. M., and J. Weinstock, Nonlinear theory of density fluctuations in turbulent plasmas, *Phys. Fluids*, *15*, 1507, 1972.

Smith, L. G., and O. Royrvik, Electron-density irregularities in the day-time equatorial ionosphere, *J. Atmos. Terr. Phys.*, *47*, 813, 1985.

St.-Maurice, J.-P., and R. Laher, Are observed broadband plasma wave amplitudes large enough to explain the enhanced electron temperatures of the high-latitude *E* region?, *J. Geophys. Res.*, *90*, 2843, 1985.

St.-Maurice, J.-P., and K. Schlegel, A theory of coherent radar spectra in the auroral *E* region, *J. Geophys. Res.*, *88*, 4087, 1983.

St.-Maurice, J.-P., K. Schlegel, and P. M. Banks, Anomalous heating of the polar *E* region by unstable plasma waves, 2, Theory, *J. Geophys. Res.*, *86*, 1453, 1981.

St.-Maurice, J.-P., C. Hanuise, and E. Kudeki, On the dependence of the phase velocity of equatorial irregularities on the polarization electric field and theoretical implications, *J. Geophys. Res.*, *91*, 13,493, 1986.

Sudan, R. N., Nonlinear theory of type I irregularities in the equatorial electrojet, *Geophys. Res. Lett.*, *10*, 983, 1983*a*.

Sudan, R. N., Unified theory of type I and type II irregularities in the equatorial electrojet, *J. Geophys. Res.*, *88*, 4853, 1983*b*.

Sudan, R. N., J. Akinrimisi, and D. T. Farley, Generation of small-scale irregularities in the equatorial electrojet, *J. Geophys. Res.*, *78*, 240, 1973.

Temerin, M., The polarization, frequency, and wavelengths of high-latitude turbulence, *J. Geophys. Res.*, *83*, 2609, 1978.

Temerin, M., and M. C. Kelley, Rocket-borne wave measurements in the dayside auroral oval, *J. Geophys. Res.*, *85*, 2915, 1980.

K. D. Baker and B. G. Fejer, Center for Atmospheric and Space Sciences, Utah State University, Logan, UT 84322.

M. C. Kelley, School of Electrical Engineering, Cornell University, Ithaca, NY 14853.

E. Kudeki, Aeronomy Laboratory, University of Illinois, 1406 West Green Street, Urbana, IL 61801.

R. F. Pfaff, NASA Goddard Space Flight Center, Code 696, Greenbelt, MD 20771.

(Received March 25, 1987;
revised August 21, 1987;
accepted August 26, 1987.)